

This is a repository copy of *Enhancing solar photovoltaic modules quality assurance through convolutional neural network-aided automated defect detection*.

White Rose Research Online URL for this paper:

<https://eprints.whiterose.ac.uk/204188/>

Version: Accepted Version

---

**Article:**

Hassan, Sharmarke and Dhimish, Mahmoud (2023) Enhancing solar photovoltaic modules quality assurance through convolutional neural network-aided automated defect detection. *Renewable Energy*. 119389. ISSN 0960-1481

<https://doi.org/10.1016/j.renene.2023.119389>

---

**Reuse**

This article is distributed under the terms of the Creative Commons Attribution (CC BY) licence. This licence allows you to distribute, remix, tweak, and build upon the work, even commercially, as long as you credit the authors for the original work. More information and the full terms of the licence here:

<https://creativecommons.org/licenses/>

**Takedown**

If you consider content in White Rose Research Online to be in breach of UK law, please notify us by emailing [eprints@whiterose.ac.uk](mailto:eprints@whiterose.ac.uk) including the URL of the record and the reason for the withdrawal request.

# Enhancing Solar Photovoltaic Modules Quality Assurance through Convolutional Neural Network-Aided Automated Defect Detection

Sharmarke Hassan\*, Mahmoud Dhimish

Laboratory of Photovoltaics, School of Physics, Engineering and Technology, University of York, York YO10 5DD, United Kingdom

\*Corresponding Author: [smh600@york.ac.uk](mailto:smh600@york.ac.uk)

## **Abstract**

Detecting cracks in solar photovoltaic (PV) modules plays an important role in ensuring their performance and reliability. The development of convolutional neural networks (CNNs) has introduced a game-changing dimension in the detection of defects in PV modules. This paper proposes an automated defect detection method for PV, by leveraging custom-designed CNN to accurately analyse electroluminescence (EL) images, identifying defects such as cracks, mini-cracks, potential induced degradation (PID), and shaded areas. The proposed system achieves a high level of validation accuracy of 98.07%, reducing manual inspection demands, enhancing quality standards, and saving costs. The system was validated in a case study for PV installations faulty with PID, where it identified all defective modules with a high degree of precision of 96.6%, surpassing existing methods. This methodology holds promise for revolutionizing PV industry quality control, improving module reliability, and supporting sustainable solar energy growth.

**Keywords:** Convolutional Neural Network; Artificial Energy; Photovoltaics; Automated Defect Detection; Electroluminescence Imaging.

## **1. Introduction**

Convolutional neural network (CNN) stands as the most prominent deep learning technique in the field of machine learning. With the advent of this computer vision-based technology, humans can now perform tasks that were previously inconceivable, such as face recognition, automatic disease diagnosis, or autonomous vehicle operation [1]. By enabling machines to interpret images and videos, CNN has significantly transformed the way individuals interact with the world, opening new possibilities for research and various applications.

As a result of learning and performing task effortlessly and intelligently, CNN can execute tasks on par with human beings. It has thus been able to deliver the promised results such as recognition of faces or objects [2], detection of objects or fraud [3], or prediction of weather [4]. Additionally, CNN suggests friends on social media by suggesting individuals who they may already know [5].

35 Moreover, CNN's ability to respond to new situations quickly and effectively is a testament to  
36 its advanced artificial intelligence (AI) capabilities. The architectures of CNN are primarily  
37 developed by experts with extensive domain knowledge, which makes it challenging for users  
38 without domain expertise to utilize them; therefore, there has been a growing interest in  
39 automating the architectures to enhance both efficiency and accessibility [6,7].

40 CNN architectures are divided into two main categories: automatic + manual tuning  
41 architectures and automated architectures [8-11]. As a result of the first category offering the  
42 extra feature of manually adjusting, it is superior to existing architectures incapable of manual  
43 tuning, even though individuals without domain knowledge of CNN prefer architectures that  
44 are designed to not require manual tuning since no adjustments are necessary.

45 Since PV modules are produced daily, it is becoming increasingly challenging to perform  
46 manual inspections to detect defects, and so the need for automated inspections has  
47 increased. Therefore, researchers have focused on developing automated inspection  
48 methods such as image processing and signal processing [12-15]. As a result, automated  
49 inspection methods have been widely studied in recent years, and many successful  
50 implementations have been reached. Despite this, the use of CNN as an automated means of  
51 defect detection has increased significantly in recent years [16,17]. However, a recent study  
52 yielded 93% accuracy when using CNN as an automated technique of defect detection<sup>18</sup>. As  
53 such, these techniques have become increasingly popular for detecting defects, with CNNs  
54 being particularly successful in this regard.

55 Consequently, the CNN detection technique has several advantages that make it superior to  
56 conventional methods. The first advantage is that CNN is capable of learning and detecting  
57 the various patterns present in EL images. As a second advantage, the CNN technique  
58 achieves excellent accuracy and saves time since manual inspection is not required, in  
59 addition to the fact that sometimes large quantities of PV are required for inspection. As a  
60 third benefit, CNN can prevent hazards since it detects different types of PV defects. Overall,  
61 the cumulative effect improves the accuracy of defect detection and the durability and  
62 performance of PV modules.

63 CNN is praised for achieving remarkable performance in a wide range of image-related tasks  
64 but suffers from several limitations about solar panel inspection. Firstly, the lack of extensive  
65 and diverse datasets is a major impediment. Current approaches often rely on datasets  
66 containing fewer than 10,000 images, limiting their ability to capture the full spectrum of real-  
67 world conditions. Consequently, training CNN models on such insufficient data may limit their  
68 capacity to accurately identify patterns and detect cracks across varying scenarios.

69 Moreover, CNNs struggle with generalization in solar panel inspection. Solar panels display a  
70 wide range of diversity in design, texture, and manufacturing processes. Additionally,  
71 environmental conditions like light intensity and soiling levels vary significantly between  
72 installations. CNN models, typically trained on specific datasets, fail to account for this  
73 diversity. Consequently, a model trained to detect cracks in one type of solar panel may fail  
74 when applied to others, as it lacks the adaptability to recognize patterns unique to different  
75 panels. Furthermore, CNNs often operate as "black boxes," lacking interpretability and

76 explain ability. This is a crucial limitation when trust and accountability are paramount. In  
77 solar panel inspection, understanding why a model classified a particular cell as cracked is  
78 vital. Incorporating interpretability and explain ability mechanisms into CNN models is  
79 essential to establish trust, ensuring reliability in critical applications.

80

81 This work represents a novel approach to automated PV defect detection techniques as it  
82 consists of two levels of inspection: the cell level inspection and the module level inspection.  
83 This is accomplished by inspecting each solar cell separately, and based on the results,  
84 determining whether the module has been accepted or rejected based on the percentage of  
85 healthy cells. In contrast, the green indicator indicates that a solar cell is healthy or accepted,  
86 while the red indicator indicates that a solar cell has been defected.

87 This is achieved by developing four different CNN architectures, and by varying the number  
88 of convolutional layers and pooling of architectures, we reach an impressive level of validation  
89 accuracy of 98.07%, which is referred to in this paper as Arch 4. The four architectures are  
90 trained using a dataset that contains images of healthy and defective solar cells. The  
91 architectures are then evaluated based on several metrics, such as accuracy, precision, recall,  
92 and specificity. The best performing architecture, Arch 4, is then used to classify the solar cells  
93 into healthy and defective categories.

94 Highlighting its uniqueness, the approach presented in the research paper stands out as the  
95 sole method with the ability to detect a diverse array of anomalies, including cracks, PID,  
96 shaded regions, and breakdowns. This distinctive capability positions the research as a  
97 pioneering endeavour, offering a comprehensive solution to quality assessment within the PV  
98 industry. The emphasis on this aspect underscores the groundbreaking nature of this work  
99 and its potential to significantly advance the field. This work stands out from the rest, offering  
100 a comprehensive solution to quality assessment within the PV industry. Its pioneering nature  
101 and potential impact make it a groundbreaking achievement in the field.

102 A notable aspect of this research is its two-level inspection strategy, which includes  
103 examinations at both the cell and module levels. By carefully assessing individual solar cells  
104 and then evaluating overall module health based on the percentage of healthy cells, this  
105 approach adds precision that greatly improves defect detection. This innovative approach  
106 addresses an evident gap in current knowledge, as previous methods focused on module-  
107 level inspections.

108 Furthermore, this research involves the optimization and customization of CNN architectures,  
109 leading to an impressive validation accuracy of 98.07% (referred to as Arch 4). This  
110 achievement reflects the research team's dedication to advancing automated inspection  
111 techniques while enhancing the methods' practicality. In summary, this research introduces  
112 an innovative approach to automated PV defect detection and validates its feasibility and  
113 effectiveness through extensive empirical testing. By offering a more detailed and precise  
114 defect analysis method, this study contributes to PV module quality control development.  
115 With an increasing demand for solar energy solutions, this research has the potential to  
116 enhance the efficiency, reliability, and sustainability of the solar energy sector.

117 **2. Materials and Methods**

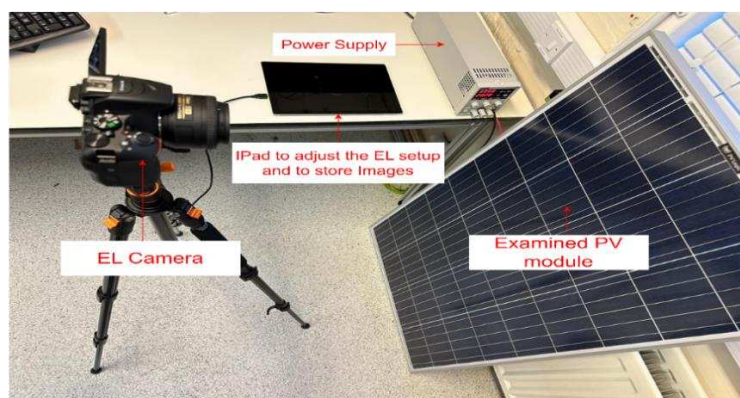
118 **2.1 EL Imaging**

119 The electroluminescence (EL) imaging technique is an effective method to inspect the  
120 performance of solar cells [19]. To achieve this, it is imperative to apply a biased current to  
121 the cell. In turn, this will cause it to glow, making it easy to detect all defects that the solar  
122 cell has, that are not visible to the naked eye [20]. Furthermore, it is a non-destructive testing  
123 method, which allows inspection of the entire cell's surface quickly and accurately.

124 Thus, in this study, a Brightspot automation imager was utilised to capture EL images, which  
125 were captured using a digital camera with a resolution of 6k x 4k pixels and a focal length of  
126 18-55mm, as shown in Figure 1(a), and the main components of Brightspot EL Imaging setup  
127 are shown in Figure 1(b). The Brightspot Automation imager was chosen due to its ability to  
128 capture high-resolution images with a wide field of view.  
129 This allows the capture of more detail and provides a better overall picture of the EL images.  
130 Additionally, the digital camera with the 6k x 4k resolution and 18-55mm focal length provides  
131 a very sharp image with a wide range of colours and contrast. In addition, the PV module was  
132 connected to a power supply to generate a biased current.



133 (a)



134 (b)

135 Figure 1. (a) EL imaging setup, (b) EL imaging components.

## 2.2 Image Segmentation

Image segmentation is a computer vision task that entails labelling specific areas of an image based on what is being displayed on the image [21]. To be precise, semantic image segmentation aims to label each pixel in an image with a class corresponding to what is being represented in that image, as the system is predicting the outcome of every pixel [22,23]. This is achieved by using supervised or unsupervised learning algorithms to detect certain features of the image and then assigning a label to each pixel based on those features. For example, these algorithms can be used to recognize objects in the image, and then label each pixel according to the object it belongs to.

The process of labelling an image pixel-by-pixel can be defined as the collection of random variables  $\{x_0, \dots, x_n\}$ . Where  $n$  represents the image's total pixels. Each element  $x_i \in L$  takes one of  $m$  discrete labels from the set  $L = \{1, \dots, m\}$ . A convolutional neural network (CNN) models a probability distribution  $Q(X|\theta, I)$  over the random variables  $X$ , where  $\theta$  represents the network parameters. Typically, this distribution is modeled as a product of independent marginals, denoted as  $Q(X|\theta, I) = \prod_i q_i(x_i|\theta, I)$  [24]. Each of these marginals represents a SoftMax probability. Each marginal  $q_i(x_i|\theta, I)$  is parameterized by a set of weights  $\theta_i$  which are learned by the CNN during training (R). The parameters  $\theta$  are learned by optimizing the network to minimize a loss function, which is a measure of the difference between the predicted and actual outputs. This functionality is presented in (1) below [24].

$$q_i(x_i|\theta, I) = \frac{\exp(f_i(x_i; \theta, I))}{z_i} \quad (1)$$

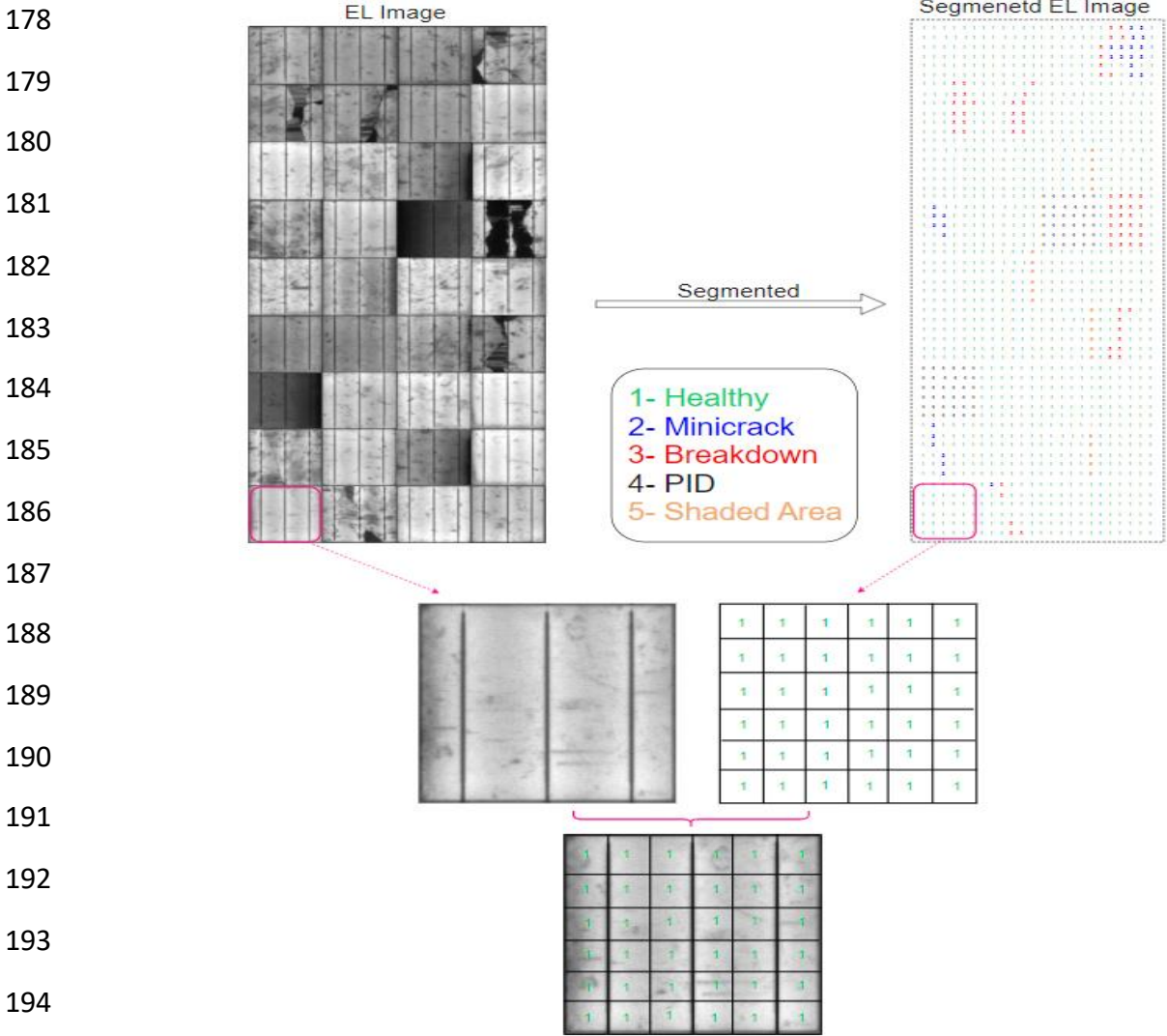
Where  $z_i = \sum_{l \in L} \exp(f_i(x_i; \theta, I))$  represents the partition function of pixel  $i$ . The function  $f_i$  represents the numerical score of the neural network.

As a result, in this study, the EL images of the PV panels were segmented into solar cells pixel, and each pixel was examined, segmented into pixels based on conditions, such as healthy, Mini crack, breakdown, PID, and shaded areas, as shown in Figure 2(a). The first pixel segment is characterized as healthy, labelled as 1, and represents every solar cell pixel with no defects. The second segment of solar cells is made up of solar cell pixels with mini cracks and is indicated by 2.

Consequently, the third segment of the solar cells are composed of solar cell pixels with major cracks or breakdowns, which can massively degrade the PV panels' output power, and it is labelled as 3 [25]. The fourth segment of the label is potential-induced degradation (PID). PID is a leading cause of module degradation and is caused by the high voltage generated between the encapsulants and the front glass surface, which is grounded through either the cell frame or the substructure, and it is labelled as 4 (PID) [26]. Lastly, is the shaded area. Shaded is represented as 5 in the colour scheme as shaded areas create uneven current distribution in the busbars, which in turn stresses the cells and consequently higher temperatures would result in power degradation [27].

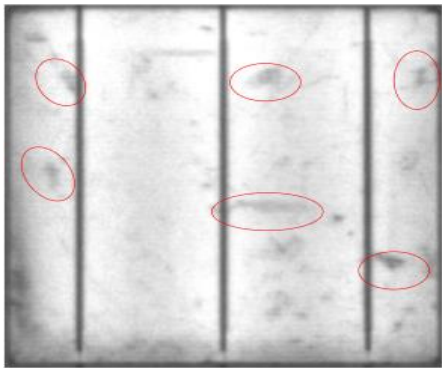
The pixels were further analysed to determine the percentage of each condition in the PV panel to assess the overall health of the solar cell. It was noted that minor blotches appeared on the solar cells, as shown in Figure 2(b). These spots appeared on the EL because of the

176 camera's calibration/resolution, and they do not have a detrimental effect on the solar cells.  
177 Hence, these spots are negligible when examining the condition of the cells.



195

196 (a)



(b)

199 Figure 2. (a) Segmentation processing of PV module EL image, (b) Minor black spots appear  
200 in the EL image of the solar cell.

### 2.3 CNN Architecture

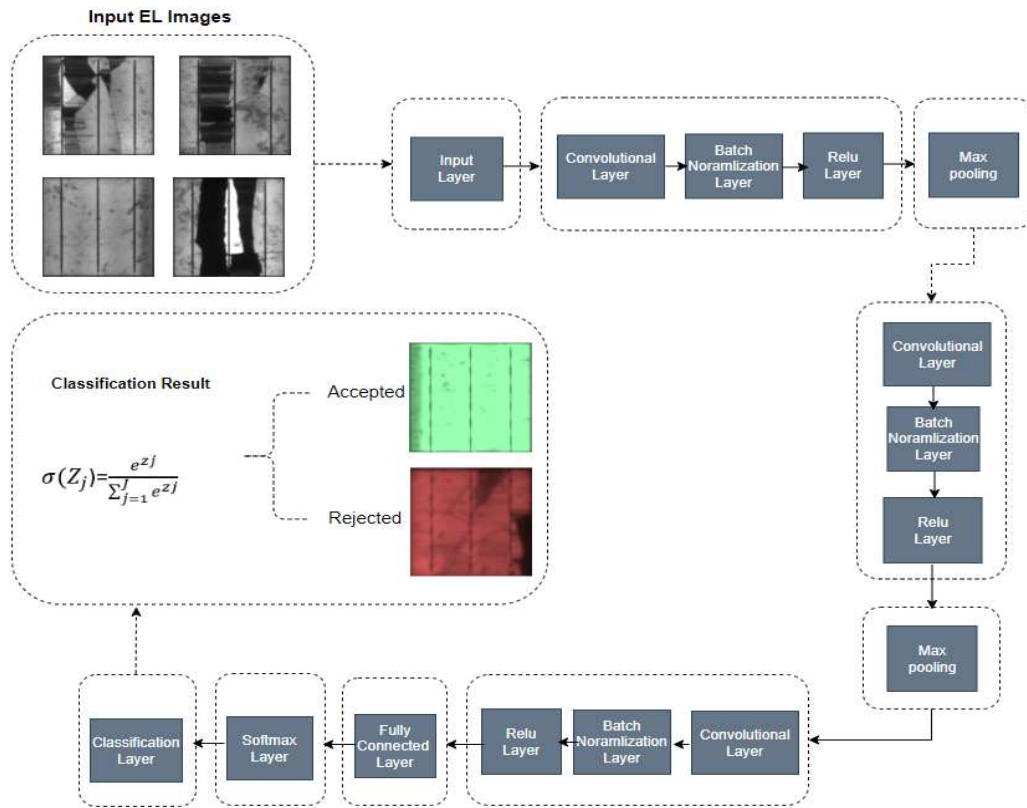
Having completed the segmentation of the image, the subsequent stage is to build a CNN architecture that is suitable for training tasks like this with a high level of validation accuracy. Therefore, there are different layers to employ to build CNN architecture, as shown in Figure 3. The first layer is the convolutional layer composed of filters that are learned during the process and are smaller in size than the actual image. This layer later is combined with an activation map. The second layer is the batch Normalization layer, and its main function is to maintain regularity and avoid excess fitting and at the same time to speed up the computation of the CNN. The Rectified Linear Unit (ReLU) is the next layer. Its main function is to remove all negative numbers and replace them with zero. The next layer is the pooling layer, which extracts values from image segments defined by kernels.

There are two methods to retrieve the value, either by using max pooling and retrieving the maximum number or by using mean pooling and computing the average. Hence, there is no universal solution, and decisions should be made during training. A fully connected layer in a neural network uses weight matrices to linearly transform input vectors and solve problems, resulting in every possible connection between input and output vectors being present. The CNN network employs the SoftMax function as the activation function in the output layer to predict a probabilistic distribution in multi-class classification problems. The last layer is the classification layer, which applies predefined rules for classifying.

Several architectures were developed from scratch, each with its own layers. As shown in Table 1, Arch 1 has two convolutional layers and mean pooling with a learning rate of 0.0001 and 20 epochs, and the key parameters of all architectures are summarized in Table 2. Arch 1 had a validation accuracy of 81.5%. Our second architecture, referred to as Arch 2, contains two convolutional layers, each with 32 filters, arranged in a connection between a normalization layer and a Relu layer. However, the unique feature of this architecture is its use of max-pooling rather than mean pooling, leading to an accuracy rate of 87.5% for validation accuracy, followed by a third architecture, Arch 3, which has three layers of convolutional layers with 32 filters and double pooling of max and mean, resulting in a validation accuracy of 93.75%. This improved accuracy of Arch 3 is attributed to the double pooling of both max and mean, which is unique to this architecture. During the construction of the architecture, the research team continuously built and tested different architectures (Arch 1-4) until Arch 4 was developed, which achieved a peak validation accuracy of 98.07%. A detailed description of Arch 4 is presented in Figure 3.

Choosing Arch 4 was based on the fact that Arch 4 was made up of two double convolutional layers with double max pooling, which resulted in a higher validation accuracy than all the other architectures. Hence, achieving a validation accuracy higher than that of Arch 4 is not feasible, since keeping the training network in place while modifying the Architecture components will drop the validation accuracy. This is because the two double convolutional layers and double max pooling provide an added depth to the network that allows it to accurately identify patterns in the data. By changing the architecture, one essentially strips away the complexity and depth of the network, which inevitably reduces its accuracy.





243

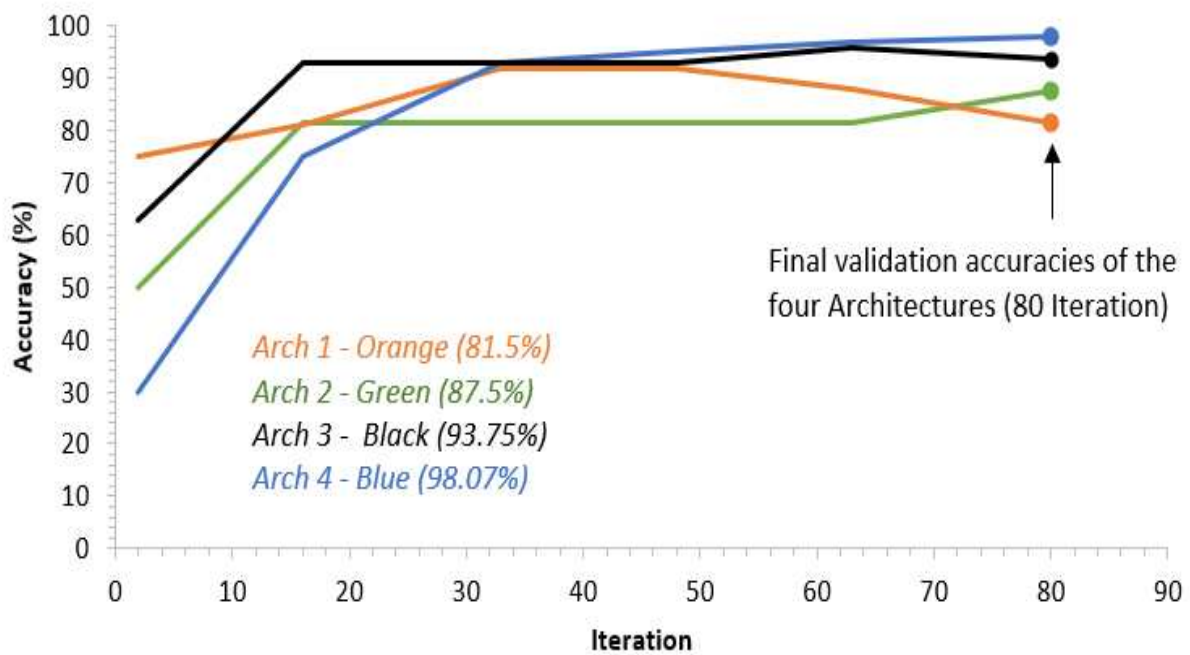
244

Figure 3. CNN Network architecture of Arch 4.

Table 1. Summary of the different architectures implemented and tested in this work.

Architecture Name	Description	Validation accuracy
Arch 1	Contains two convolutional layers of 32 filters connected to a normalization layer and a Relu layer by means of mean pooling, with initial input pixels of 227x227x3 pixels.	81.5%
Arch 2	Contains two convolutional layers of 32 filters connected to a normalization layer and a Relu layer by means of max pooling, with initial input pixels of 227x227x3 pixels.	87.5%
Arch 3	With an initial input size of 227x227x3 pixels, this convolutional layer contains three layers of 32 filters connected to a normalization layer and a Relu layer through a double pooling of max and mean.	93.75%
Arch 4	Three convolutional layers containing 32 filters with an initial input size of 227x227x3 pixels is connected through a double max pooling to a normalization layer and a ReLU layer.	98.07%

245 In developing a CNN architecture for solar cell inspection, adjusting parameters such as the  
 246 number of epochs, learning rate, and validation accuracy was a major challenge [28]. To  
 247 overcome this challenge, the team started with a learning rate of 0.01 and 10 epochs for the  
 248 first CNN network, gradually increasing the learning rate to 0.0001 and epochs to 20, resulting  
 249 in a maximum validation accuracy of 81.5% for Arch 1. Replicating the mean pooling of Arch  
 250 1 with the max pooling of Arch 2 improved the validation accuracy to 87.5%. Adding three  
 251 convolution layers with max-mean and max-max pooling for Arch 3 and Arch 4, respectively,  
 252 improved the accuracy to 93.75% and 98.07%, respectively, with 20 epochs and a learning  
 253 rate of 0.01. Figure 4 compares the validation accuracy of Arch 1 to 4.



254  
255

Figure 4. Validation accuracies of the four different CNN networks.

Table 2. Summary of CNN input parameters for (Arch 1-4).

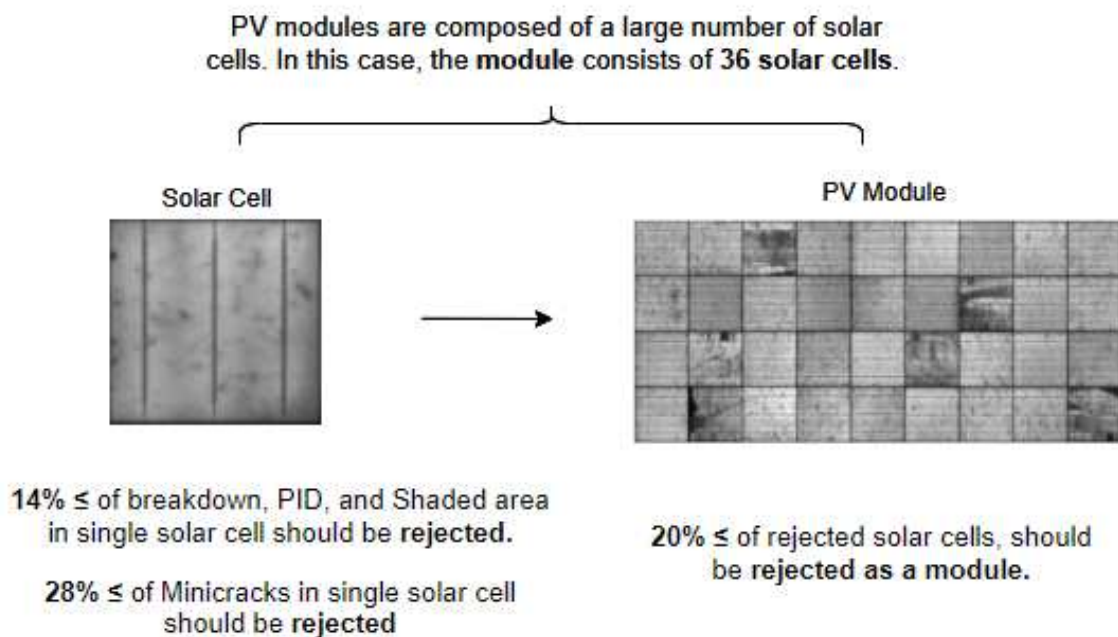
Parameter	Value	Parameter	Value
Convolutional layers	32 Filters	Epochs	20
Filter size	3,3	Image input Size	227x227x3 Pixels
Mini batch size	16	Learn rate drop factor	0.1
Validation frequency	16	Initial learn Rate	0.0001
Solver	Sgdm	random rotation (Degree)	-90, 90

## 2.4 Decision Making Criterion

256 The algorithm is heavily dependent on CNN's decision-making process. Accordingly, the  
257 system is required to analyse two distinct outputs in order to make an accurate  
258 determination, namely the PV module and its constituent PV cells. Therefore, the PV cells in  
259 a solar panel are components of the PV module, as the module is composed of individual cells.  
260 CNN detects and analyses PV cells within the PV module to accurately determine the  
261 efficiency of the PV module. This information can then be used to optimize the solar panel's  
262 performance. Consequently, CNN will examine each cell separately and determine whether it  
263 will be accepted or rejected based on standard quality shown in Figure 5, based on standard  
264 criteria, with green indicating acceptance and red indicating rejection.  
265

266 In the next step, a prediction is made on the module level. Each module consists of many solar  
267 cells. Therefore, the CNN network will determine whether the PV module is accepted or  
268 rejected based on the analysis of each solar cell individually. Essentially, if more than 20% of  
269 the solar cells within a module are predicted to be rejected, that module will be considered  
270 rejected. Figure 5 shows detailed standard quality. This prediction is based on the data  
271 gathered from each individual solar cell and the comparison of it to the standard quality. This  
272 prediction is further analysed to determine the status of the entire module.

273 In this criterion, prior understanding has been considered, which suggests that if 14% of cells  
274 exhibit significant defects, such as breakdown, shading, or PID, it can have a considerable  
275 influence on cell performance, leading to a more than 10% reduction in power output  
276 [27,29,30]. However, the impact of the mini crack is relatively minor compared to other  
277 defects such as PID and the shaded area, which has twice the impact of the mini crack  
278 [15,31,32]. So, it depends on the user's established criteria. This is exemplified by the fact that  
279 Quality standards on PV assembly lines may vary, providing adjustable parameters.



280  
281

Figure 5. Standard quality criteria.

## 282 **3. Results**

283 The assessment of the CNN network put forward in this study can be broken down into two  
284 distinct sections, in light of its dual-component structure. Specifically, the first component of  
285 validation is conducted at the level of individual cells, while the second component focuses  
286 on the module level, as the predicted output of the cells directly impacts the overall status of  
287 the modules. This approach to validation serves to ensure the reliability and efficacy of the  
288 CNN network under consideration while accounting for the complex interactions between its  
289 constituent elements.

### 290 **3.1 Cell Level Prediction**

291 During the solar cell inspection process, each solar cell is examined separately by the trained  
292 CNN network. This is done by examining all its pixels and then categorizing them as accepted  
293 or rejected. This is done to ensure that each cell meets the quality standards, as shown in  
294 Figure 5.

295 Accordingly, four different cells with varying conditions were examined. As shown in Figure  
296 6, the first cell was a healthy cell free of defects. In turn, a CNN network was then employed  
297 to examine each pixel independently to determine if there are any defects. Based on the  
298 findings, it was predicted that the cell was accepted since it met the standard quality,  
299 intended to have a cell with less than 14% of defects considered healthy, hence it was  
300 displayed as green. In the second case, the CNN network predicted that the cell is unhealthy  
301 since it presents a shaded area, and thus rejected it since more than 14% of the cell is  
302 defective, resulting in it displaying as red.

303 Due to the defects in the third cell, the CNN predicted it as rejected since most pixels were  
304 defective, and it was illustrated as red. A fourth cell, which presented a mini crack, was  
305 deemed to be healthy by the CNN network based on the standard quality of a mini crack of  
306 28%, which differs significantly from the standard quality for other defects, thus 17% of the  
307 mini cracks are rated as healthy and displayed as green.

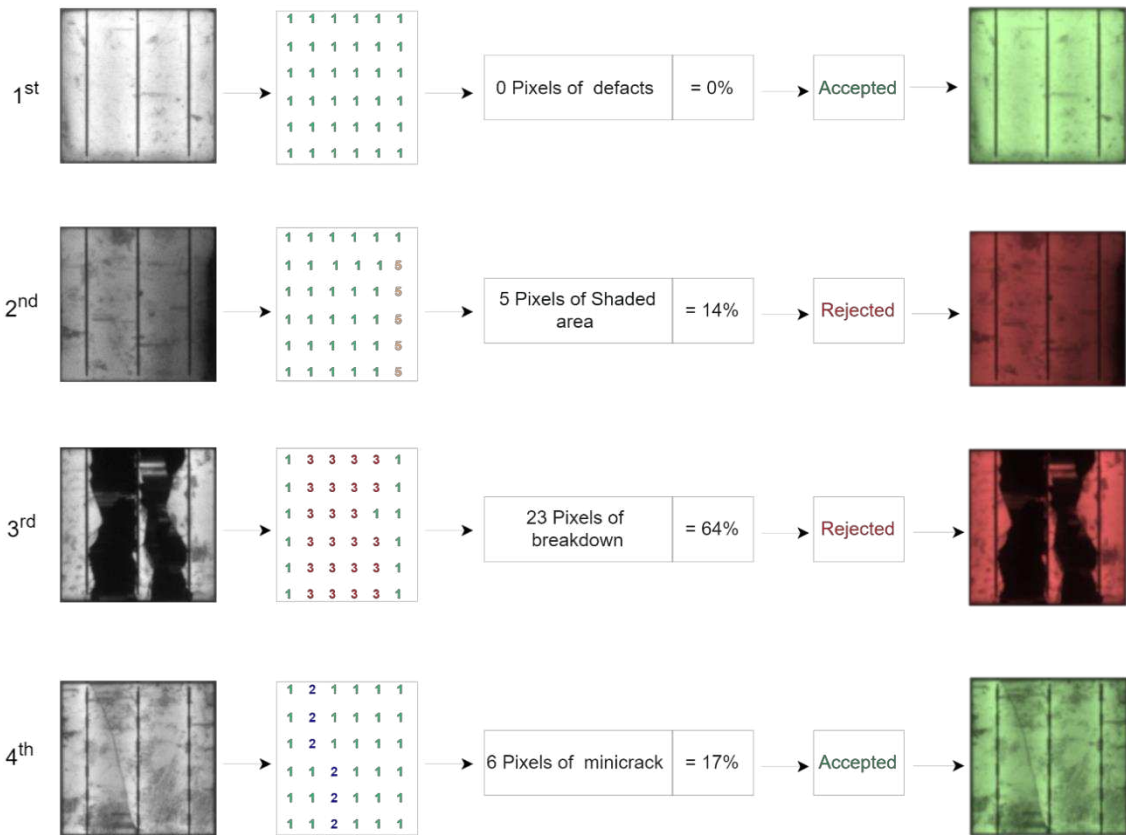
308 Consequently, the CNN network has shown the capability of detecting different defects in  
309 solar cells and predicting them precisely. This makes it a trustworthy way to inspect solar cells,  
310 and it could be used on all manufacturing assembly lines. This will contribute to the  
311 production of high-quality solar cells and reduce production costs. Moreover, it would help  
312 minimize the reliance on manual labour and facilitate in production of a higher quantity of  
313 solar cells with improved efficiency. As a result, this could have a significant impact on the  
314 renewable energy sector and help lower the cost of renewable energy sources.

### 315 **3.2 Module Level Prediction**

316 Within this section, the study addresses CNN's predictive capabilities at the module level by  
317 assessing individual solar cells and subsequently determining the module's prediction based  
318 on established quality standards shown in Figure 5, achieved through an independent  
319 examination of each cell. This approach allows for the evaluation of the CNN's performance  
320 concerning quality standards and facilitates the identification of potential flaws in the solar

321 modules that can be attributed to individual cells. Examining each cell individually aids in  
 322 identifying potential issues that might otherwise be overlooked during module inspection.

323

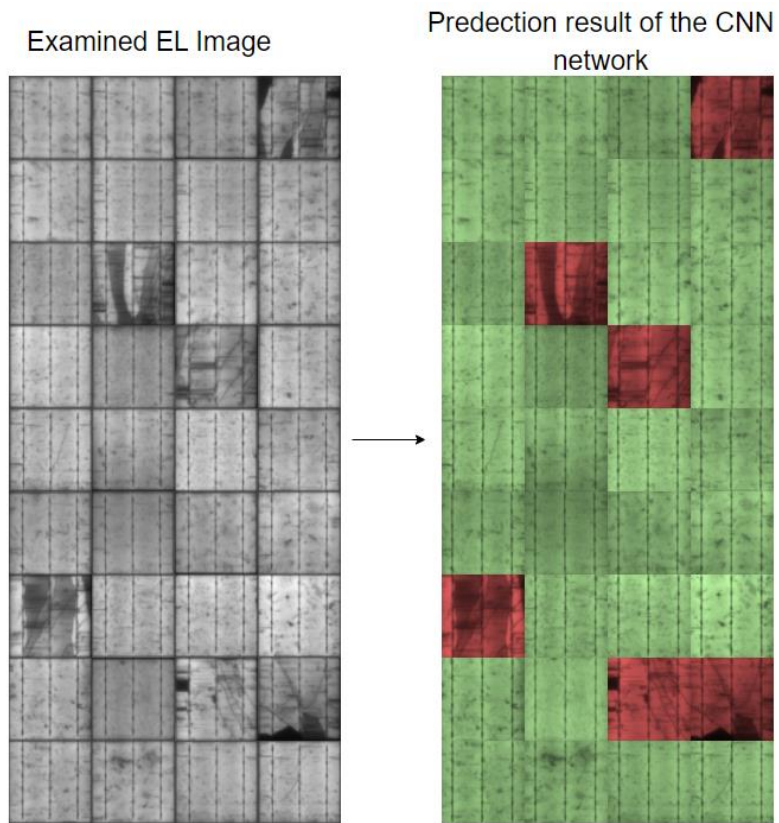


324

325 Figure 6. Cell level prediction (Mix of accepted and rejected cases).

326 To conduct the prediction, a PV module was examined and processed within a CNN network.  
 327 As shown in Figure 7, the module is comprised of 36 solar cells, which were assessed  
 328 separately using the CNN network. Based on CNN's assessment, 6 of the 36 solar cells on this  
 329 module were deemed defective, equalling 17% of the module. As the percentage of defects  
 330 is less than 20% of the standard quality rate, the system is referred to as a healthy PV module.  
 331 Consequently, the system successfully predicted the PV module's health, while maintaining a  
 332 relatively high-quality rating. This means that the CNN network accurately detected defective  
 333 solar cells and distinguished them from healthy ones. As a result, it accurately assessed the  
 334 overall health of the PV module and determined that it meets the standard quality rate.

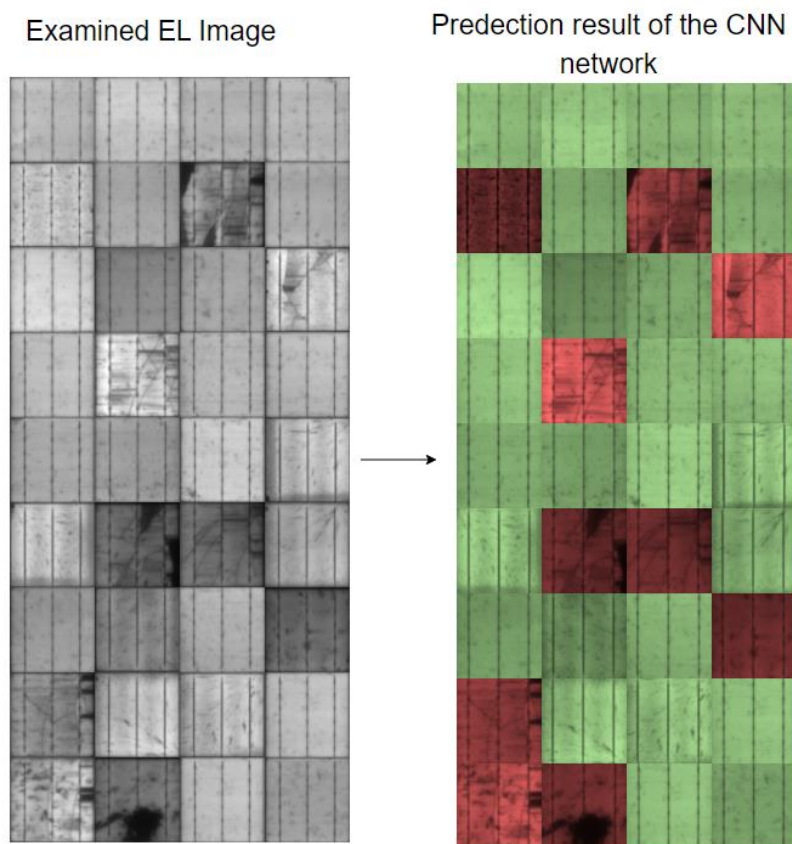
335 A second PV module was employed to mark the prediction with a CNN network, as shown in  
 336 Figure 8. According to the CNN analysis, the CNN network predicted that 10 of 36 solar cells  
 337 of the module were defective, accounting for 28% of the total solar cells. As this defect rate  
 338 surpasses the standard quality rate of 20%, the module was predicted to be rejected. The  
 339 standard quality rate is based on the expected performance of a PV module, so if the defect  
 340 rate surpasses that, it is likely that the module will not be able to meet the necessary  
 341 standards for use. As a result, it is rejected.



342

343

Figure 7. Module level prediction (accepted case).



344

345

Figure 8. Module level prediction (rejected case).

### 3.3 Diverse EL imaging angles

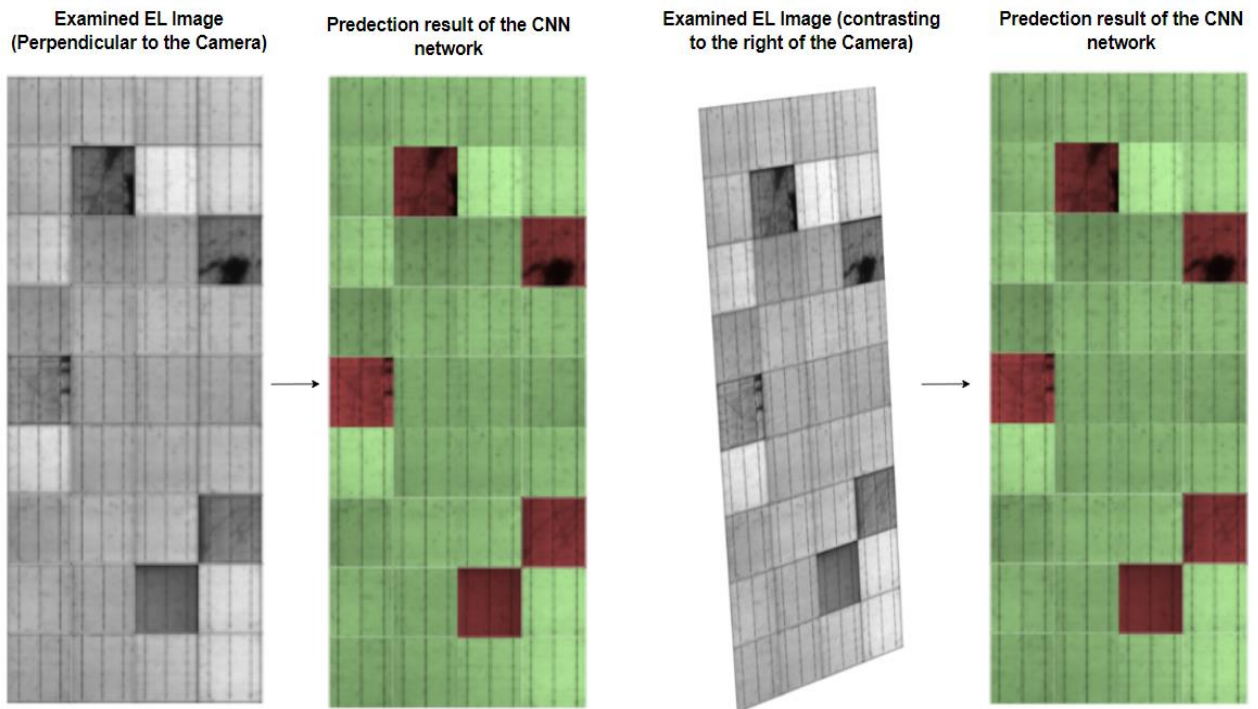
346 Normally, EL imaging takes place by pointing the camera perpendicular to the PV module,  
347 however, there may be instances when the camera can't be positioned perpendicular to the  
348 PV module due to space limitations, or PV modules are installed on a tilted roof, and therefore  
349 it is imperative to take EL images at an angle. In such cases, the camera should be positioned  
350 as close as possible to the perpendicular angle and the EL images should be adjusted  
351 accordingly to ensure accuracy.  
352

353 Considering these factors, three different EL images taken with the same PV module at various  
354 angles were examined. as shown in Figure 9. A first look at Figure 9(a) shows the conventional  
355 method of capturing EL images; the EL camera is positioned perpendicular to the PV module  
356 being examined and the CNN is predicted as being normal since there has been no change in  
357 configuration. In addition, the PV module examined during EL camera capture had a tendency  
358 to contrast to the right as illustrated in Figure 9(b) and the system predicted the same result  
359 as the conventional method.

360 Furthermore, the third exam was conducted by contrasting the EL camera to the left of the  
361 Examining PV module using the same camera configuration, as shown in Figure 9(c). However,  
362 the system predicted the same results regardless of the camera angle. As a result, it can be  
363 concluded that the EL camera capture was able to achieve consistent results, regardless of  
364 the orientation of the PV module or the camera configuration. This indicates that the EL  
365 camera has excellent consistency in capturing light and that it can accurately detect the  
366 orientation of the PV module without any deviations. Furthermore, it also shows that the EL  
367 camera is reliable for capturing light from different angles and with different camera  
368 configurations.

369 Considering the three different angles in which the proposed CNN tool was examined, it made  
370 the same prediction, as shown in Figure 9, indicating that the proposed tool has the capacity  
371 to work from a variety of angles, eliminating the need to take the perpendicular angle to  
372 utilize the tool. This highlighted the power of the proposed CNN tool to reliably perform its  
373 task with great accuracy, regardless of the input angle. The high quality of this PV module  
374 serves as a testament to the effectiveness of the CNN network, demonstrating its accuracy in  
375 predicting defects with a high degree of accuracy. The results of this study further confirm  
376 that CNN networks are highly effective at detecting defects in PV modules, providing a reliable  
377 and accurate method for quality assurance. It also confirms the potential of AI for use in the  
378 solar industry and other applications.

379 Additionally, this proposed tool has the benefit of examining different solar cells with a variety  
380 of busbar technologies, since most modern solar cells are constructed using various busbar  
381 (BB) designs, such as 3BB, 4BB and 5BB, so this proposed tool will be able to examine and  
382 identify any defects in the solar cell, whether it is a 3BB, 4BB or 5BB. Moreover, this  
383 instrument can accurately assess not just the standard 3BB, 4BB and 5BB busbar technology,  
384 but also any other type of busbar technology that may be employed in modern solar cells,  
385 allowing it to detect any possible defects. This makes it a great tool for ensuring the highest  
386 quality standards for solar cells and their production.

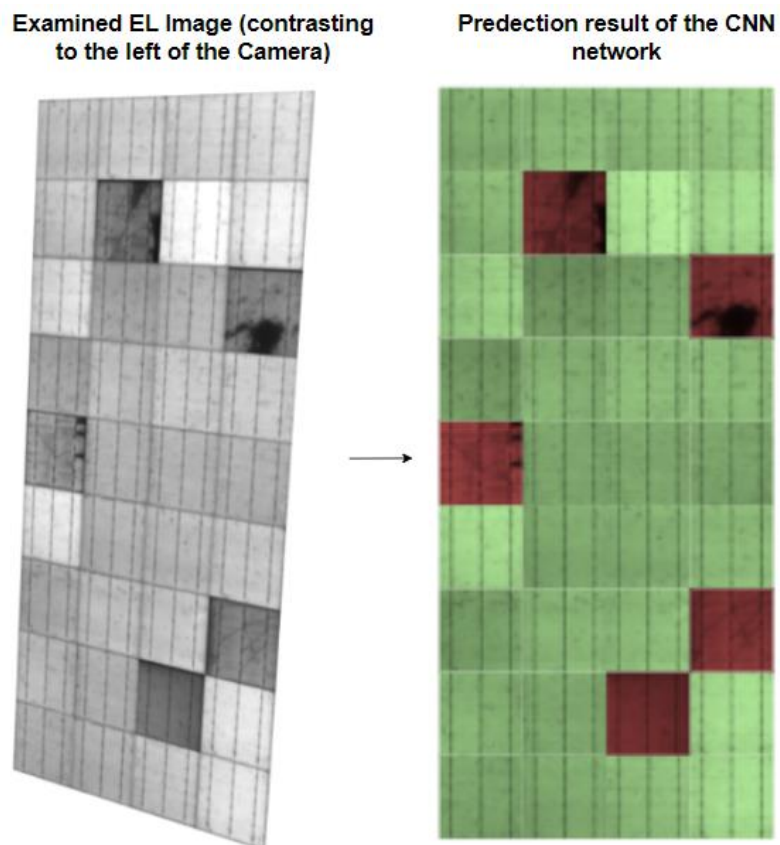


387

388

(a)

(b)



389

390

(c)

391 Figure 9. Predicting PV module level based on different imaging angles. (a) Perpendicular to  
 392 the camera, (b) Contrasting to the right of camera, (c) Contrasting to the left of camera.



393 **3.4 Case Study**

394 With the proposed CNN network, the main application is to assess the large scale of PV  
395 systems with minimal effort and within a short timeframe, along with a high degree of  
396 accuracy. Therefore, a case study was conducted for a PV system. The case study was  
397 conducted to validate the CNN network's accuracy. Additionally, it was intended to assess the  
398 usefulness of the network in terms of identifying potential faults in the PV system and  
399 providing guidance in terms of maintenance and optimization. According to Figure 10, the PV  
400 string consists of nine polycrystalline silicon PV modules connected in series, and Table 3  
401 summarises the string's main electrical parameters.



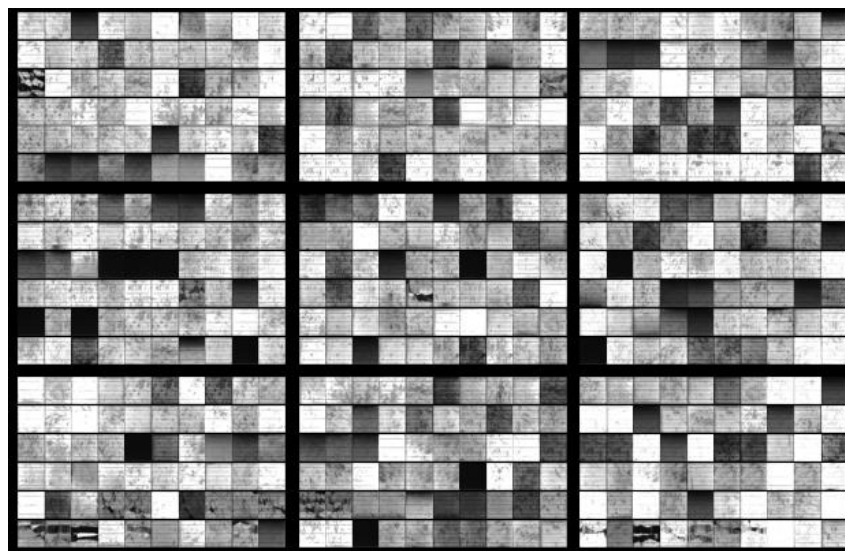
402 Figure 10. Examined PV system

403 Table 3. Electrical parameters of the second examined PV string at STC conditions.

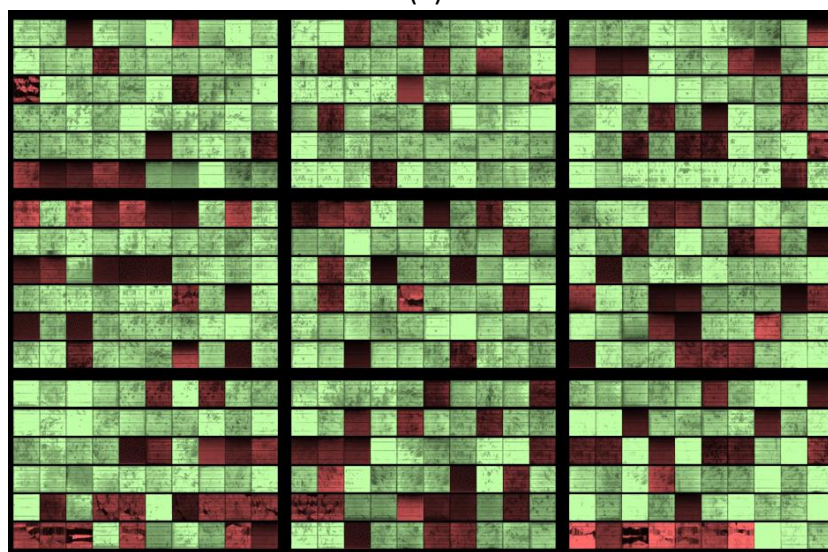
Parameter	Value
Power at maximum power point ( $P_{MPP}$ )	1950 W
Current at maximum power point ( $I_{MPP}$ )	7.55 A
Voltage at maximum power point ( $V_{MPP}$ )	258.3 V
Short circuit current ( $I_{SC}$ )	8.05 A
Open circuit voltage ( $V_{OC}$ )	331.2 V

404 The EL images of the PV modules were initially captured as illustrated in Figure 11(a), followed  
405 by an analysis of all the EL images so that the system can classify them according to the  
406 standard qualities shown in Figure 5. Consequently, the CNN network classified the solar cells  
407 into green for those without defects and red for those with defects as shown in Figure 11(b).  
408 Therefore, all 9 modules were predicted as rejected since the PV string is defective due to PID  
409 (potential-induced degradation).

410 As a result, the proposed system can be an extremely useful tool for large-scale PV  
411 installations by classifying the solar cells based on standard criteria with the assistance of the  
412 CNN, the proposed tool can accurately detect defective cells with high precision. This can  
413 significantly reduce the cost of large-scale PV installations by reducing the need for manual  
414 inspection and maintenance. Furthermore, the system can also be used to identify any  
415 potential problems before they occur, thus further reducing the overall costs associated with  
416 a large-scale PV installation.



(a)



(b)

418 Figure 11. (a) EL image of the Modules, (b) Predicted result of the modules from the CNN  
419 network.  
420

421 An additional parameter to consider is how well the model performs in terms of predicting  
 422 correctly or incorrectly for the data set under consideration, which is done by creating a  
 423 confusion matrix table for the data set. The confusion matrix in Table 4 illustrates the results  
 424 of the case study, which is made up of 540 solar cells, of which 385 are healthy while 155 are  
 425 defective. Based on this, the accuracy and precision of the model are calculated using  
 426 equations (1) and (2) to assess its performance, respectively.

427 Specifically, it was found that the accuracy of the model was 95.5%, which indicates that the  
 428 model correctly classified 95.5% of all solar cells based on their health or crackability In this  
 429 instance, the precision was 96.6%, which means that 96.6% of the solar cells that were  
 430 actually defective were categorised as defective by the model, indicating that the CNN model  
 431 was very accurate and precise in its prediction of the solar cells.

432 **Table 4.** Confusion matrix of the developed CNN model “Net4”.

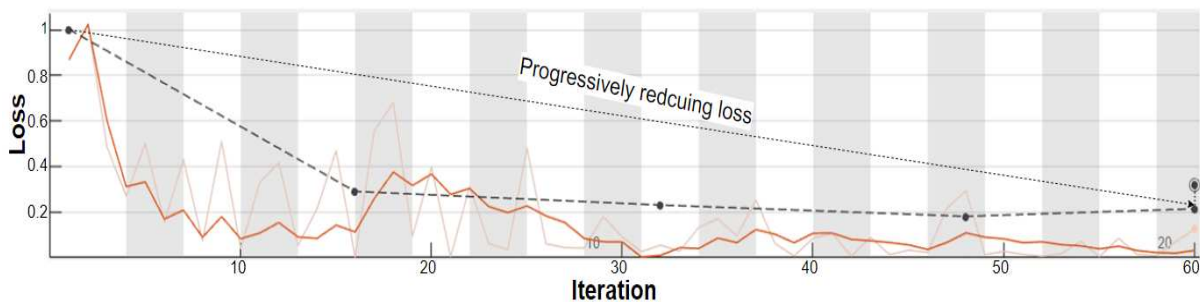
		Actual Value	
		Actual No Cracks	Actual Cracks
Predicted Value	Predicted No Cracks	374	11
	Predicted Cracks	13	142

433 
$$Accuracy = \frac{TP+TN}{TP+TN+FP+FN} = \frac{374+142}{374+142+13+11} = 95.5\% \quad (2)$$

434 
$$Precision = \frac{TP}{TP+FP} = \frac{374}{374+13} = 96.6\% \quad (3)$$

435 The selection of an appropriate loss function for CNN models holds a great deal of significance  
 436 as it quantifies the disparity between the predicted output and the actual ground truth data.  
 437 The CNN model is carefully trained with adjustments to critical parameters to minimize the  
 438 loss function and enhance performance, with the goal of minimising the loss function as part  
 439 of the training process. It is designed to enhance the model's ability to accurately predict the  
 440 loss function and to significantly increase its overall performance through this optimization  
 441 process.

442 As shown in Figure 12, which presents Arch 4, we observe a desirable loss graph with two  
 443 lines: red for training loss and blue for validation loss. The convergence and decrease of both  
 444 lines indicate that the model reduces prediction errors. Initially, the model showed a slightly  
 445 higher loss, but with continuous training, the loss steadily decreased toward zero. This results  
 446 in effective learning and a remarkable reduction in loss and error.



447  
 448 **Figure 12.** Arch 4 CNN network learning Loss vs learning iterations (epochs).  
 449

450 **3.4 Sensitivity analysis**

451 In the following section, an analysis of sensitivity regarding two pivotal parameters, the data  
452 split ratio and the number of training epochs, is presented. Sensitivity analysis serves to  
453 discern the effects of parameter variations on the system's performance.

454 The study explored different data split ratios, allocating data for training and validation  
455 purposes in varying proportions: 50% training - 50% validation, 55% training - 45% validation,  
456 60% training - 40% validation, 65% training - 35% validation, 70% training - 30% validation,  
457 75% training - 35% validation and 80% training - 20% validation. Subsequently, the accuracy  
458 of the system was evaluated under each configuration. Results from this sensitivity analysis  
459 indicated that the configuration employing an 80% training - 20% validation split exhibited  
460 the highest accuracy. This allocation appeared to strike an optimal balance between training  
461 data volume and validation data representativeness. Deviating from this ratio, either by  
462 increasing or decreasing the validation data proportion, was observed to result in decreased  
463 accuracy. This finding underscores the significance of the data split ratio as a critical factor in  
464 optimising system performance.

465 Additionally, the sensitivity analysis delved into the influence of training epochs by varying  
466 the number of epochs employed during the training process. Six different configurations were  
467 examined, involving 5, 10, 15, 20, 25 and 30, epochs, as shown in Figure 13. Accuracy  
468 measurements were recorded for each configuration. The analysis demonstrated that the use  
469 of 20 training epochs yielded the highest accuracy. Importantly, fewer epochs resulted in a  
470 decline in accuracy due to inadequate model convergence, while increasing the number of  
471 epochs beyond a certain threshold yielded diminishing returns and a corresponding drop in  
472 accuracy. This outcome highlights the necessity for a judicious selection of the number of  
473 training epochs during model training.

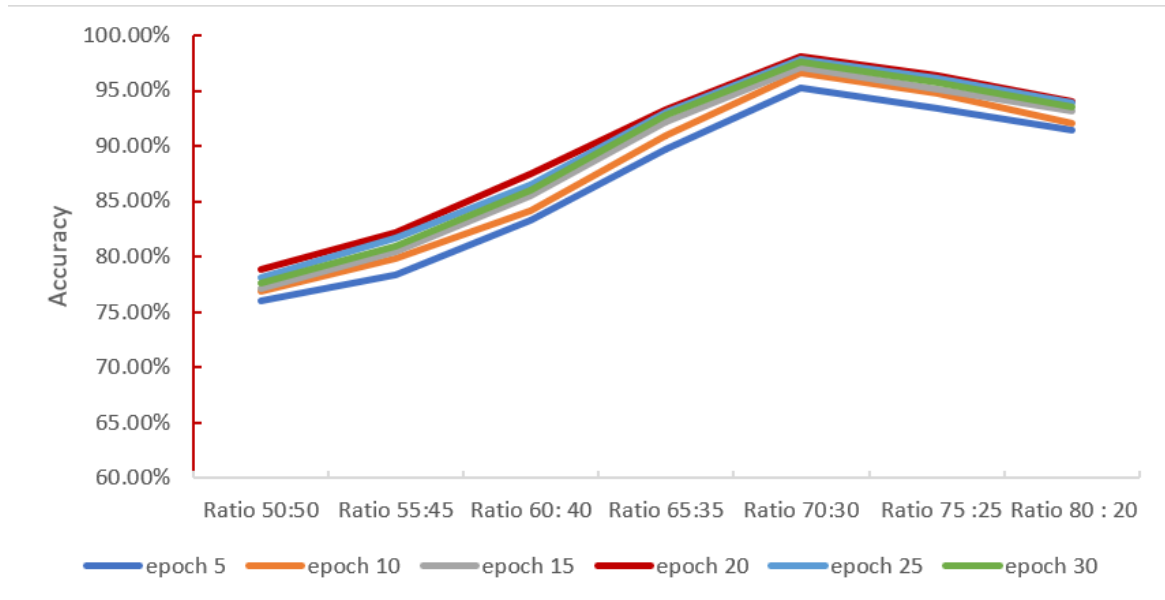
474 In order to provide further clarity regarding the effects of data split ratios and epochs,  
475 confusion matrices are presented in the tables 5. These matrices offer a comprehensive  
476 breakdown of the system's performance under each configuration, allowing for a more  
477 detailed understanding of how variations in these parameters impact the system's  
478 classification and prediction capabilities.

479 **Table 5** Sensitivity analysis of two parameters (data split ratio and epoch).

	<b>Epoch 5</b>	<b>Epoch 10</b>	<b>Epoch 15</b>	<b>Epoch 20</b>	<b>Epoch 25</b>	<b>Epoch 30</b>
Ratio 50:50	76.03%	76.93%	77.18%	78.89%	78.10%	77.63%
Ratio 55:45	78.43%	79.90%	80.50%	82.23%	81.66%	81.01%
Ratio 60:40	83.33%	84.19%	85.53%	87.52%	86.47%	85.96%
Ratio 65:35	89.77%	90.96%	92.22%	93.33%	93.02%	92.86%
Ratio 70:30	95.24%	96.64%	97.13%	98.07%	97.86%	97.55%

Ratio 75:25	93.37%	94.83%	95.21%	96.43%	96.11%	95.79%
Ratio 80:20	91.43%	92.09%	93.21	94.04%	93.88%	93.55%

480



481

482

Figure 13. Accuracy of the sensitives of Epochs vs data split ratio.

483

484

485

486

487

488

489

In summary, the sensitivity analysis conducted in this study underscores the pronounced influence of data split ratios and the number of training epochs on the system's accuracy. Specifically, a data split ratio of 80% training - 20% validation and 20 training epochs produced the most favourable results. It is worth noting that the optimal values for these parameters may vary depending on the specific dataset and problem domain. Consequently, a deliberate and empirical approach to parameter selection is essential for the optimization of model performance.

490

#### 4. Comparative Analysis

491

492

493

494

495

496

497

498

To gauge the feasibility of our proposed method, the research compared the results to several existing automated PV defect detection methods [18, 33-35] currently available in the PV industry. Table 6 provides a summary of the comparison. Several recent automated PV defect detection techniques utilizing the CNN architecture [18,33,34]. Nevertheless, it shares a comment limitation – the existing methods can only inspect at the cell level, and not at the module level as this work does. Additionally, a distinction based on the cell level is the existing methods can only detect cracks, regardless of their severity. However, it is insufficient to detect other defects such as PIDs and shaded areas.

499

500

501

502

Besides these automated PV defect detection methods, there are also automated PV defect detection methods that are based on CNN architectures that are not developed but rely instead on transfer learning to detect PV defects. This is done by using pre-trained CNN architectures that can be tweaked without affecting their genetic composition. Recently, a

503 study has been conducted to inspect PV module level using pre-trained AlexNet architecture  
 504 [35]. This method differs in that it is used to inspect conventional PV images, as opposed to  
 505 EL image. As a result, detecting defects such as PIDs or minor cracks that are not visible in  
 506 conventional PV images will become increasingly challenging.

507 In this study, an automated method was developed for detecting PV defects at both the cell  
 508 and module levels. This implies that module inspection is based on a visual assessment of the  
 509 individual solar cells and can be accepted or rejected according to the percentage of healthy  
 510 solar cells in each module. Moreover, the proposed method is capable of detecting defects  
 511 such as cracks, PIDs, and shaded areas, unlike all other methods that are currently available.  
 512 As a result, this system can be utilized in two different manners. First the system can be  
 513 applied for cell-level inspection in PV assembly lines to inspect solar cells manufactured on  
 514 the assembly line. The second application is that module-level inspection can be used to  
 515 assess large-scale PV modules thereby minimizing manual labour and saving time while  
 516 maintaining a high level of accuracy.

517 In this way, this proposed tool has proven to be highly accurate for the assessment of solar  
 518 cells and PV modules and is the only tool available currently that can assess both the cells and  
 519 modules simultaneously, in real-time, within a specified timeframe. Furthermore, this  
 520 proposed tool can be used to examine PV modules at different angles, for example by taking  
 521 an EL image from either the left or right side of the module and obtaining the same prediction  
 522 regardless of the angle. This is since the proposed tool utilises CNN, which has the ability to  
 523 detect and recognise features in images regardless of their orientation. Additionally, the  
 524 proposed tool can be used to examine many PV systems, or planted PV systems, in a timely  
 525 and convenient manner. Furthermore, the tool can provide an efficient and cost-effective way  
 526 to analyse and compare the performance of numerous PV systems, both installed and  
 527 planned.

528 **Table 6.** Comparison between our developed network against several recently develop solar  
 529 cell cracks detection algorithms [18, 33-35].

Ref.	Year of Study	Solar cell cracks detection description	Inspection level		Inspected Defects		
			Cell level	Module level	Cracks	PID	Shaded area
[33]	2018	MCCNN: Multi-channel convolutional neural networks are used by connecting several channels of CNNs to a fully connected layer and fusing them together using a random forest model.	✓	X	✓	X	X
[35]	2020	AlexNet-CNN: a method based on CNN transfer					

		learning to detect cracks with pre-trained AlexNet networks	X	✓	✓	X	X
[18]	2019	Light CNN: A CNN architecture composed of four convolutional layers and a regularization scheme based on L2 weights has been developed from scratch	✓	X	✓	X	X
[34]	2022	Gradient Guided Architecture: Lightweight CNN architectures were developed, by connecting gradient guided filter tuning to two convolutional layers and two fully connected layers.	✓	X	✓	X	X
This work	2023	In this study, A CNN architecture was developed from scratch using four different architectures and by varying the number of convolution layers and changing the pooling level to double maximum pooling, we achieved the highest validation accuracy.	✓	✓	✓	✓	✓

## 530 **5. Conclusions**

531 In conclusion, this study presents an innovative automated PV defect detection method,  
532 driven by a robust CNN architecture with an impressive validation accuracy of 98.07%.  
533 The methodology involves a comprehensive assessment of EL images at both the cell and  
534 module levels, enabling thorough evaluation of PV module health. This system exhibits  
535 remarkable versatility, accurately identifying various defects such as cracks, minicracks,  
536 PIDs, and shaded areas.

537 The results of this research are promising. The CNN-based model consistently provided  
538 precise predictions across diverse solar cell and PV module conditions. The evaluation  
539 culminated in a case study involving nine PV modules connected in series, affirming the  
540 system's ability to reliably distinguish between healthy and defective modules with a high  
541 level of precision, as evidenced by the detailed confusion matrix analysis. However, it is  
542 imperative to acknowledge certain limitations inherent to this study. Future research  
543 endeavours must address these constraints to further enhance the proposed method's  
544 applicability. Notably, improving model interpretability is crucial, and this can be achieved

545 through visualization techniques like Attention mechanisms and Saliency Maps, shedding  
546 light on the rationale behind the model's decision-making processes.

547 Furthermore, performance optimization is paramount. Lightweight CNN architectures,  
548 quantization, and pruning techniques can significantly accelerate inference speed,  
549 particularly when handling larger PV modules. Robustness testing under varying  
550 environmental conditions is also a future avenue to explore, ensuring the model's  
551 reliability in real-world scenarios. The integration of this automated defect detection  
552 system into PV manufacturing assembly lines holds tremendous potential, enabling real-  
553 time defect identification and contributing to higher-quality solar cell production. Future  
554 research should extend the scope of defect detection to include novel defect types and  
555 refine the model's capacity to discern subtler defects.

556 Moreover, the comparative study conducted in this research underscores the system's  
557 superiority over existing automated PV defect detection methods. While prior approaches  
558 have been limited to cell-level inspection and the detection of specific defect types, the  
559 proposed CNN-based system can inspect both cells and modules simultaneously, in real-  
560 time, within agreed-upon time frames. This emphasizes its high accuracy and efficiency.  
561 In sum, this research serves as a foundational step toward a transformative tool in the PV  
562 industry, offering precise and efficient defect detection. By addressing these limitations  
563 and exploring these future directions, researchers and industry professionals can ensure  
564 the continued evolution and effectiveness of the CNN-based system, thereby advancing  
565 the reliability and performance of solar energy systems while reducing costs and  
566 improving productivity.

567

## 568 **Data Availability Statement**

569 The dataset generated and analysed in this study may be available from the corresponding  
570 author S.H. on reasonable request.

## 571 **Acknowledgements**

572 This research was funded by the School of Physics, Engineering, and Technology at the  
573 University of York under the project titled "Practical Experimentation on the Deployment of  
574 Solar Roads".

## 575 **Author contributions**

576 Both authors discussed the organization and the content of the manuscript. --. performed the  
577 experiments, prepared figures, and wrote the main manuscript text. --. validated the  
578 experimental results and revised the manuscript. Both authors have approved the manuscript  
579 before submission.

## 580 **Competing interests**

581 The author declares no competing interests.



## 582 References

- 583 1. Li, Z., Liu, F., Yang, W., Peng, S. & Zhou, J. A Survey of Convolutional Neural Networks:  
584 Analysis, Applications, and Prospects. *IEEE Trans Neural Netw Learn Syst* **33**, 6999–  
585 7019 (2022).
- 586 2. Coskun, M., Ucar, A., Yildirim, O. & Demir, Y. Face recognition based on convolutional  
587 neural network. *Proceedings of the International Conference on Modern Electrical and*  
588 *Energy Systems, MEES 2017* **2018-January**, 376–379 (2017).
- 589 3. Momeny, M. *et al.* Grading and fraud detection of saffron via learning-to-augment  
590 incorporated Inception-v4 CNN. *Food Control* **147**, 109554 (2023).
- 591 4. Zhang, L., Huang, Z., Liu, W., Guo, Z. & Zhang, Z. Weather radar echo prediction  
592 method based on convolution neural network and Long Short-Term memory  
593 networks for sustainable e-agriculture. *J Clean Prod* **298**, 126776 (2021).
- 594 5. Pan, N., Yao, W. & Li, X. Friends Recommendation Based on KBERT-CNN Text  
595 Classification Model. *Proceedings of the International Joint Conference on Neural*  
596 *Networks* **2021-July**, (2021).
- 597 6. Salama, W. M. & Aly, M. H. Deep learning in mammography images segmentation  
598 and classification: Automated CNN approach. *Alexandria Engineering Journal* **60**,  
599 4701–4709 (2021).
- 600 7. Jalali, S. M. J., Ahmadian, S., Kavousi-Fard, A., Khosravi, A. & Nahavandi, S. Automated  
601 Deep CNN-LSTM Architecture Design for Solar Irradiance Forecasting. *IEEE Trans Syst*  
602 *Man Cybern Syst* **52**, 54–65 (2022).
- 603 8. Sun, Y., Xue, B., Zhang, M., Yen, G. G. & Lv, J. Automatically Designing CNN  
604 Architectures Using the Genetic Algorithm for Image Classification. *IEEE Trans Cybern*  
605 **50**, 3840–3854 (2020).
- 606 9. Kolar, D., Lisjak, D., Pajak, M. & Gudlin, M. Intelligent Fault Diagnosis of Rotary  
607 Machinery by Convolutional Neural Network with Automatic Hyper-Parameters  
608 Tuning Using Bayesian Optimization. *Sensors* **2021**, Vol. 21, Page 2411 **21**, 2411  
609 (2021).
- 610 10. Bakhshi, A., Noman, N., Chen, Z., Zamani, M. & Chalup, S. Fast Automatic  
611 Optimisation of CNN Architectures for Image Classification Using Genetic Algorithm.  
612 *2019 IEEE Congress on Evolutionary Computation, CEC 2019 - Proceedings* 1283–1290  
613 (2019) doi:10.1109/CEC.2019.8790197.
- 614 11. Atteia, G., Abdel Samee, N., El-Kenawy, E. S. M. & Ibrahim, A. CNN-Hyperparameter  
615 Optimization for Diabetic Maculopathy Diagnosis in Optical Coherence Tomography  
616 and Fundus Retinography. *Mathematics* **2022**, Vol. 10, Page 3274 **10**, 3274 (2022).
- 617 12. Dhimish, M. & Mather, P. Ultrafast High-Resolution Solar Cell Cracks Detection  
618 Process. *IEEE Trans Industr Inform* **16**, 4769–4777 (2020).

- 619 13. Qian, X., Li, J., Cao, J., Wu, Y. & Wang, W. Micro-cracks detection of solar cells surface  
620 via combining short-term and long-term deep features. *Neural Networks* **127**, 132–  
621 140 (2020).
- 622 14. Parikh, H. R. *et al.* Solar Cell Cracks and Finger Failure Detection Using Statistical  
623 Parameters of Electroluminescence Images and Machine Learning. *Applied Sciences*  
624 *2020, Vol. 10, Page 8834* **10**, 8834 (2020).
- 625 15. Dhimish, M. & Holmes, V. Solar cells micro crack detection technique using state-of-  
626 the-art electroluminescence imaging. *Journal of Science: Advanced Materials and*  
627 *Devices* **4**, 499–508 (2019).
- 628 16. Rahman, M. R. *et al.* CNN-based Deep Learning Approach for Micro-crack Detection  
629 of Solar Panels. *2021 3rd International Conference on Sustainable Technologies for*  
630 *Industry 4.0, STI 2021* (2021) doi:10.1109/STI53101.2021.9732592.
- 631 17. Ahmad, A. *et al.* Photovoltaic cell defect classification using convolutional neural  
632 network and support vector machine. *IET Renewable Power Generation* **14**, 2693–  
633 2702 (2020).
- 634 18. Akram, M. W. *et al.* CNN based automatic detection of photovoltaic cell defects in  
635 electroluminescence images. *Energy* **189**, 116319 (2019).
- 636 19. Hassan, S. & Dhimish, M. Review of Current State-of-the-Art Research on Photovoltaic  
637 Soiling, Anti-Reflective Coating, and Solar Roads Deployment Supported by a Pilot  
638 Experiment on a PV Road. *Energies* *2022, Vol. 15, Page 9620* **15**, 9620 (2022).
- 639 20. Dhimsih, M. & Mather, P. Development of Novel Solar Cell Micro Crack Detection  
640 Technique. *IEEE Transactions on Semiconductor Manufacturing* **32**, 277–285 (2019).
- 641 21. Sultana, F., Sufian, A. & Dutta, P. Evolution of Image Segmentation using Deep  
642 Convolutional Neural Network: A Survey. *Knowl Based Syst* **201–202**, 106062 (2020).
- 643 22. Kim, W., Kanazaki, A. & Tanaka, M. Unsupervised Learning of Image Segmentation  
644 Based on Differentiable Feature Clustering. *IEEE Transactions on Image Processing* **29**,  
645 8055–8068 (2020).
- 646 23. Mahani, G. K. *et al.* Bounding Box Based Weakly Supervised Deep Convolutional  
647 Neural Network for Medical Image Segmentation Using an Uncertainty Guided and  
648 Spatially Constrained Loss. *Proceedings - International Symposium on Biomedical*  
649 *Imaging* **2022-March**, (2022).
- 650 24. Liu, X., Song, L., Liu, S. & Zhang, Y. A Review of Deep-Learning-Based Medical Image  
651 Segmentation Methods. *Sustainability* *2021, Vol. 13, Page 1224* **13**, 1224 (2021).
- 652 25. Aghaei, M. *et al.* Review of degradation and failure phenomena in photovoltaic  
653 modules. *Renewable and Sustainable Energy Reviews* **159**, 112160 (2022).

- 654 26. Dhimish, M. & Tyrrell, A. M. Power loss and hotspot analysis for photovoltaic modules  
655 affected by potential induced degradation. *npj Materials Degradation* 2022 6:1 **6**, 1–8  
656 (2022).
- 657 27. Dhimish, M. & Lazaridis, P. I. An empirical investigation on the correlation between  
658 solar cell cracks and hotspots. *Scientific Reports* 2021 11:1 **11**, 1–11 (2021).
- 659 28. Garbin, C., Zhu, X. & Marques, O. Dropout vs. batch normalization: an empirical study  
660 of their impact to deep learning. *Multimed Tools Appl* **79**, 12777–12815 (2020).
- 661 29. Dhimish, M., D’Alessandro, V. & Daliento, S. Investigating the Impact of Cracks on  
662 Solar Cells Performance: Analysis Based on Nonuniform and Uniform Crack  
663 Distributions. *IEEE Trans Industr Inform* **18**, 1684–1693 (2022).
- 664 30. Dhimish, M., Holmes, V., Mehrdadi, B. & Dales, M. The impact of cracks on  
665 photovoltaic power performance. *Journal of Science: Advanced Materials and Devices*  
666 **2**, 199–209 (2017).
- 667 31. Dhimish, M., Holmes, V., Dales, M. & Mehrdadi, B. Effect of micro cracks on  
668 photovoltaic output power: case study based on real time long term data  
669 measurements. *Micro Nano Lett* **12**, 803–807 (2017).
- 670 32. Dhimish, M. Micro cracks distribution and power degradation of polycrystalline solar  
671 cells wafer: Observations constructed from the analysis of 4000 samples. *Renew*  
672 *Energy* **145**, 466–477 (2020).
- 673 33. Ying, Z., Li, M., Tong, W. & Haiyong, C. Automatic Detection of Photovoltaic Module  
674 Cells using Multi-Channel Convolutional Neural Network. *Proceedings 2018 Chinese*  
675 *Automation Congress, CAC 2018* 3571–3576 (2019) doi:10.1109/CAC.2018.8623258.
- 676 34. Hussain, M., Chen, T., Titrenko, S., Su, P. & Mahmud, M. A Gradient Guided  
677 Architecture Coupled With Filter Fused Representations for Micro-Crack Detection in  
678 Photovoltaic Cell Surfaces. *IEEE Access* **10**, 58950–58964 (2022).
- 679 35. Zyout, I. & Oatawneh, A. Detection of PV Solar Panel Surface Defects using Transfer  
680 Learning of the Deep Convolutional Neural Networks. 1–4 (2020)  
681 doi:10.1109/ASET48392.2020.9118384.